Center for Turbulence Research
Proceedings of the Summer Program 1992

Isotropy of small scale turbulence

By R. A. Antonia[1] AND J. Kim[2]

The degree to which local isotropy is satisfied has been examined using direct numerical simulations for a fully developed channel flow. Attention is mainly given to the high wavenumber part of vorticity and temperature derivative spectra. The ratio of these spectra and their isotropic values depends on the particular quantity considered, the departure from isotropy being more pronounced for the temperature derivative than for the vorticity. When the Kolmogorov-normalized wavenumber is sufficiently large, isotropy is satisfied provided the (Kolmogorov-normalized) mean strain rate is sufficiently small. This result appears to be independent of the quantity considered and of the Reynolds number.

1. Introduction

The concept of local isotropy has been of central importance to the theory of turbulence and continues to attract significant attention in turbulence, as can be gleaned, for example, from the compendium of papers in the A. N. Kolmogorov commemorative issue of the *Proceedings of the Royal Society* (1991). The concept implies that the small scales become statistically independent from the large scales or, perhaps more pertinently, from any orientation effects or bias introduced by the mean shear. This implication and related questions, for example, "is local isotropy achievable only at large Reynolds numbers?" or "do departures from local isotropy persist irrespectively of the Reynolds number?", are issues which continue to preoccupy, perhaps fascinate, turbulence researchers.

Before the previous questions can be adequately addressed, there is first the need to decide how best to measure "local isotropy". This is not a straightforward task given that there is a plethora of tests which can be applied (e.g. Monin and Yaglom, 1975; Mestayer, 1982) and that different tests may have different levels of sensitivity (e.g. Antonia *et al.*, 1986). Not unrelated to these difficulties is the issue of whether the word "local" is interpreted to signify "in physical space", as originally intended by Kolmogorov (1941) or whether it is given a spectral interpretation. If the first of these interpretations is adopted, the available evidence, which includes atmospheric data at quite large turbulence Reynolds numbers, appears to point fairly unambiguously to a departure from local isotropy (e.g. Antonia *et al.*, 1986; Sreenivasan, 1991). This departure appears to be especially emphasized in statistics, e.g. mean squared values and skewnesses of spatial derivatives of the temperature fluctuation

1 Department of Mechanical Engineering, University of Newcastle, N.S.W., 2308, Australia
2 NASA-Ames Research Center, Moffett Field, CA, 94035

(e.g. Sreenivasan et al., 1979; Sreenivasan and Tavoularis, 1980). The second interpretation allows the focus to be on high wavenumbers or small scales (e.g. Van Atta, 1991; Antonia *et al.*, 1986); with the caveat that there must be non-local interactions between small and large wavenumbers (e.g. Domaradzky and Rogallo, 1991; Brasseur, 1991). This arguably provides a better framework for testing local isotropy than seems possible under the first interpretation. It is worth underlining that while the practical applications which follow from the first interpretation of the concept are well known, the spectral interpretation is not without practical significance. For example, the measurement of spatial velocity and temperature derivatives with parallel hot wires requires their separation to be selected appropriately. This is not straightforward and the analysis (Wyngaard, 1969) which provides a possible correction for the spectral attenuation of the derivative spectrum relies on local isotropy.

Regardless of which interpretation is chosen, it is important to select turbulence quantities which are representative of the small scale structure when testing for local isotropy. In this context, velocity and temperature fluctuations could be less effective than their derivatives. Direct numerical simulations (DNS) can provide more reliable data for spatial derivatives than measurements. DNS data in a turbulent channel flow have been used (Antonia *et al.*, 1991; Antonia and Kim, 1992) to test for local isotropy using both the physical space and spectral interpretations of the concept. The first paper (Antonia *et al.*, 1991) showed that mean squared velocity derivative values approximately satisfied isotropy only as the channel centerline is approached, a result which appears consistent with Durbin and Speziale's (1991) conclusion that the dissipation rate tensor cannot be isotropic when the mean strain rate is not zero. The second paper (Antonia and Kim, 1992) focused mainly on the high wavenumber part of velocity and pressure spectra; the results adequately supported local isotropy in a flow region characterized by relatively small mean strain rates. There was no attempt, however, to quantify the dependence on the mean strain rate. The present investigation extends the previous work in two important ways. It focuses on quantities (the three spatial temperature derivatives and the three components of the vorticity vector) which may have stronger contributions from the small scale structure than simply velocity and scalar fluctuations. It also attempts to relate the degree of local isotropy to the mean strain rate.

In this paper, u_i, θ, and ω_i denote the velocity, temperature, and vorticity fluctuations, respectively, the subscript i (i= 1, 2, 3) denoting the streamwise ($i = 1$), wall-normal ($i = 2$), and spanwise ($i = 3$) directions.

2 Distributions of $\overline{\theta_{,i}^2}$ and $\overline{\omega_i^2}$

Isotropy requires that the three components of $\overline{\theta_{,i}^2}$, where $\theta_{,i} \equiv \partial\theta/\partial x_i$, and $\overline{\omega_i^2}$ are equal. Figure 1 shows that this is approximately satisfied as the centerline of the channel is approached. The presentation in Figure 1 clearly highlights the strong anisotropy which exists in the wall region. Note that $\overline{\theta_{,2}^2}$ and $\overline{\omega_3^2}$ clearly dominate near the wall. There is also reasonable similarity in the shapes of the component distributions of $\overline{\theta_{,i}^2}$ and those of $\overline{\omega_i^2}$ except for the near-wall increase of $\overline{\omega_1^2}$, the mean

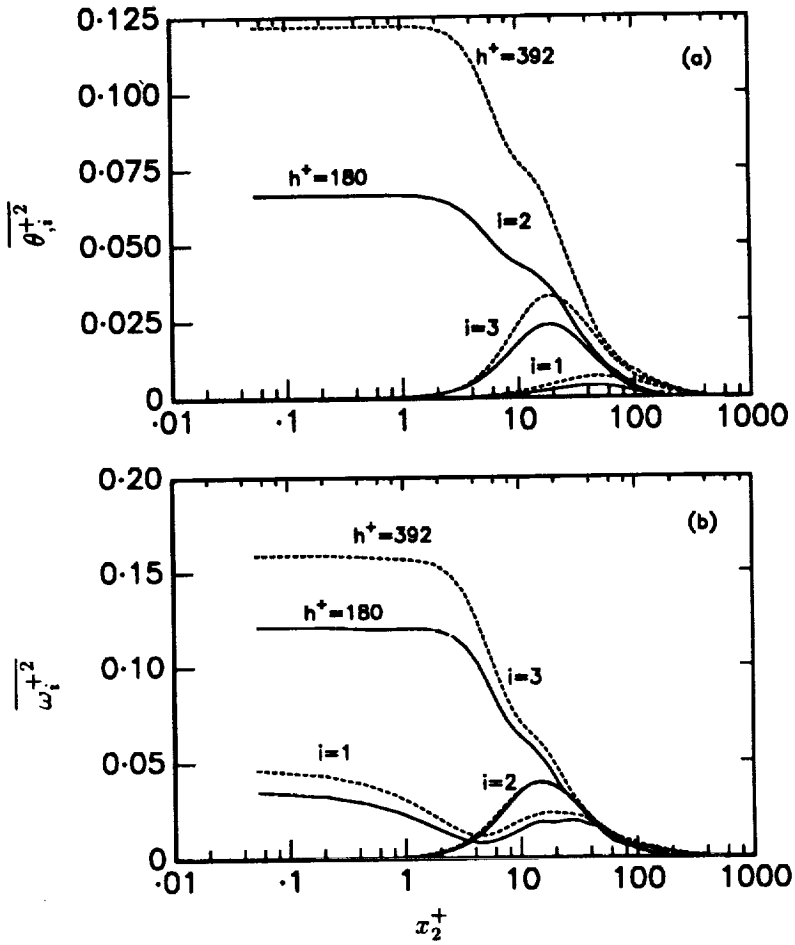

FIGURE 1. Distributions across the channel of the mean square values of the temperature derivatives and vorticity components. (a) $\overline{\theta^2_{,i}}$; (b) $\overline{\omega_i^2}$.

square longitudinal vorticity. The transport equation for $\overline{\theta^2_{,i}}$ was first written by Corrsin (1953) who compared it with the transport equation for $\overline{\omega^2}$; while the two equations can be cast in similar forms, Corrsin noted that there are apparently significant differences (due mainly to the solenoidal nature of ω_i, viz. $\nabla \cdot \omega_i \equiv 0$ or $\omega_{i,i} \equiv 0$ and the lamellar nature of $\theta_{,i}$, viz. $\nabla \times \theta_{,i} \equiv 0$).

Figure 1 also underlines the significant Reynolds number dependence in the wall region of almost all the quantities that are plotted. Apart from $\overline{\omega_2^2}$, which is virtually unaffected, the remaining quantities are increased as h^+ increases. In the sublayer, the major increases are exhibited by $\overline{\omega_3^{+2}}$ (15%), $\overline{\omega_1^{+2}}$ (32%) and $\overline{\theta_{,2}^{+2}}$ (92%). The increases in $\overline{\omega_1^{+2}}$ and $\overline{\omega_3^{+2}}$ reflect the increased stretching of the streamwise and spanwise vortices; speculatively, this stretching may increase the frequency (and amplitude) of excursions of hot fluid away from the wall and cold fluid towards the

wall, thus accounting for the increase in $\overline{\theta_{,2}^{+2}}$.

An effective method of assessing the departure from isotropy of $\theta_{,i}^2$ or ω_i^2 is to examine invariant maps (Lumley and Newman, 1977; Lee and Reynolds, 1985) of the anisotropy tensors corresponding to these quantities, the information displayed on these maps being independent of the choice of co-ordinate axes. The temperature dissipation anisotropy tensor which corresponds to $\theta_{,i}^2$ may be defined as

$$t_{ij} = \alpha \frac{\overline{\theta_{,i}\theta_{,j}}}{\overline{\epsilon_\theta}} - \frac{1}{3}\delta_{ij} \tag{1}$$

where $\overline{\epsilon}_\theta = \alpha\overline{\theta_{,i}\theta_{,i}}$ is the average temperature dissipation (α is the thermal diffusivity). The second and third variants of t_{ij} are given by

$$II = -\frac{1}{2}t_{ij}t_{ji} \tag{2}$$

$$III = \frac{1}{3}t_{ij}t_{jk}t_{ki} \tag{3}$$

and all the states that characterize t_{ij} are identifiable on a plot of $-II$ vs III, as shown in Figure 2a. Similarly, the vorticity anisotropy tensor may be defined as

$$v_{ij} = \frac{\overline{\omega_i\omega_j}}{\overline{\omega^2}} - \frac{1}{3}\delta_{ij}, \tag{4}$$

and its second and third invariants are given by expressions analogous to (2) and (3). The AIM for v_{ij} was presented in Figure 7c of Antonia *et al.* (1991). It is reproduced in Figure 2b to allow comparison with the AIM (anisotropy invariant map) of Figure 2a.

At the wall, the only component of $\overline{\epsilon}_\theta$ is $\alpha\overline{\theta_{,2}^2}$ so that the top right cusp of the AIM, with co-ordinates (2/27, 1/3), represents the one-component state of t_{ij}. As x_2^+ increases through the sublayer, the data points lie very close to the upper boundary of the AIM which represents the two-component state of t_{ij} (Figure 1 shows that $\overline{\theta_{,1}^2}$ remains small by comparison to $\overline{\theta_{,2}^2}$ and $\overline{\theta_{,3}^2}$). In the buffer region, the invariants II_t and III_t approach the left "axisymmetric" boundary ($A_t \equiv -1$) of the AIM. In the outer part of the channel, the trend is towards the isotropic state ($II_t = III_t = 0$).

Figures 2a and 2b indicate a close similarity between the invariants of t_{ij} and v_{ij} in the buffer and outer regions of the channel. In particular, along the left axisymmetric boundary, which Lee and Reynolds (1985) describe as disk-like turbulence, two components are nearly equal ($\overline{\theta_{,2}^2} \simeq \overline{\theta_{,3}^2}$, $\overline{\omega_2^2} \simeq \overline{\omega_3^2}$) while the third ($\overline{\theta_{,1}^2}$ or $\overline{\omega_1^2}$) is somewhat smaller than the other two. There are, however, marked differences between Figure 2a and Figure 2b in the near-wall region, reflecting the different boundary conditions for t_{ij} and v_{ij}. At the wall, the one-component t_{ij} state corresponds to the two-component v_{ij} state. The rod-like behavior of vorticity (right axisymmetric boundary in Figure 2b) appears to correspond to a two-component state for the temperature dissipation.

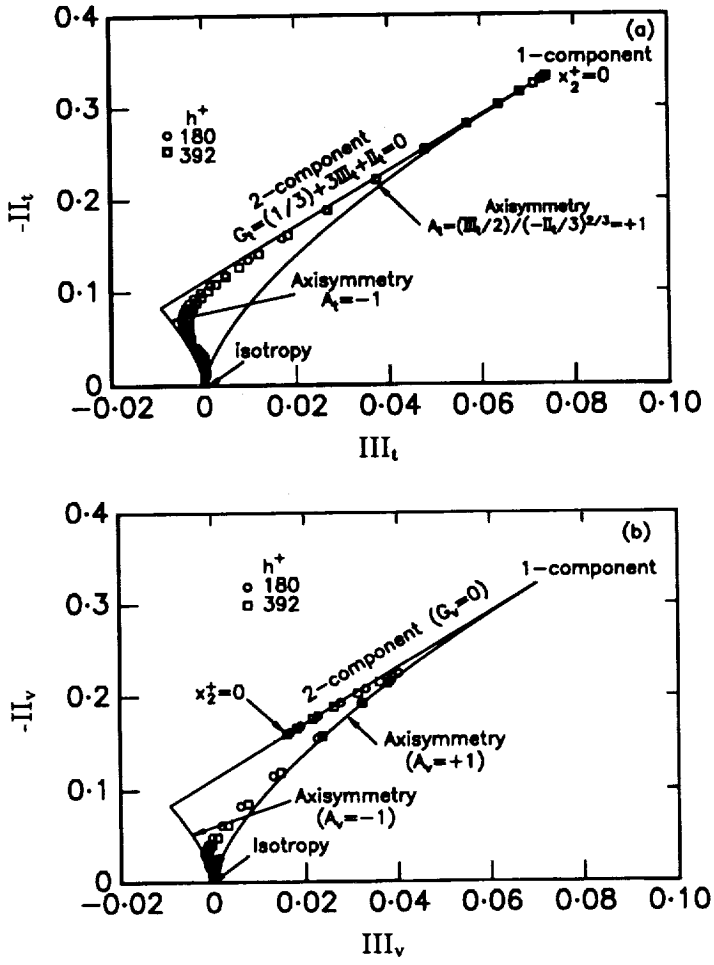

FIGURE 2. Anisotropy invariant map of temperature dissipation and vorticity. (a) $\overline{\theta_{,i}^2}$; (b) $\overline{\omega_i^2}$.

3 Spectra of ω_i and $\theta_{,i}$

The comparison between the high wavenumber part of vorticity spectra and the corresponding isotropic calculation is a useful way of assessing the degree of isotropy of the small scale structure. Since vorticity is, like velocity, solenoidal ($\omega_{i,i} \equiv 0$, $u_{i,i} \equiv 0$), isotropic relations between two-point vorticity correlations are the same as the corresponding relations between two-point velocity correlations. Using Batchelor's (1953) notation,

$$g = f + \frac{r}{2}\frac{\partial f}{\partial r} \tag{5}$$

where g and f are the lateral and longitudinal correlations respectively and r is the magnitude of the separation between the two points, the Fourier transform of (5) obviously applies to both velocity and vorticity fields. It is convenient here to

consider spectra in terms of k_3, the wavenumber in the spanwise direction. The isotropic relations for either the vorticity or velocity spectra may be written as follows

$$\phi_{\omega_1}(k_3) = \phi_{\omega_2}(k_3) = \frac{1}{2}\left(\phi_{\omega_3} - k_3\frac{d\phi_{\omega_3}}{dk_3}\right) \tag{6}$$

$$\phi_{u_1}(k_3) = \phi_{u_2}(k_3) = \frac{1}{2}\left(\phi_{u_3} - k_3\frac{d\phi_{u_3}}{dk_3}\right) \quad . \tag{7}$$

The spectra of ω_1, ω_2 and ω_2 are shown in Figure 3 for two flow locations (data for $h^+ = 392$ only are presented). The asterisk denotes normalization by Kolmogorov scales (length $\eta = \nu^{3/4}\bar{\epsilon}^{-1/4}$ and velocity $u_\kappa = \nu^{1/4}\bar{\epsilon}^{1/4}$). At the channel centerline, ϕ_{ω_1} and ϕ_{ω_2} are virtually identical at all k_3^*, as required by the first equality in (6). They are also in close agreement with the calculation given by the right side of (6). By contrast to Figure 3a, the results at $x_2^+ = 15$ (Figure 3b) show that, except at the crossing point, ϕ_{ω_1} is significantly different from ϕ_{ω_2}. The latter distribution seems to asymptote towards the isotropic calculation, Eq. (6), at sufficiently large values of k_3^*.

It is possible that the logarithmic scale on the ordinate of Figure 3 may mask small departures from isotropy. To overcome this difficulty, the ratio of the DNS spectral density to that obtained from Eq. (6) has been calculated at several x_2^+ values and plotted using a linear scale in Figure 4. Note there is a significant region of the channel for which the ratio may be assumed to be close to 1. In the case of ω_1, this approximation has an uncertainty of about $\pm 20\%$ when $x_2^+ \gtrsim 74$. For ω_2, the approximation is satisfied to about $\pm 5\%$ for $x_2^+ \gtrsim 15$. The sharp increase in the ratio at the largest values of k_3^* is spurious and can be ignored. In order to ascertain whether the spectral ratio used in Figure 4 is sensitive to departures from isotropy, the ratio was computed, using DNS data for isotropic turbulence (Rogallo, private communication). The results in Figure 5 [shown for ϕ_{ω_2} and ϕ_{u_2}; the isotropic calculations are based on $\phi_{\omega_1}(k_1)$ and $\phi_{u_1}(k_1)$] suggest that the sensitivity is adequate (better than $\pm 10\%$; the waviness in Figure 5 is a result of fitting to the ω_1 and u_1 spectra and is therefore artificial).

The isotropic relation between the temperature derivative spectra is given by (e.g. Van Atta, 1977; Browne *et al.*, 1983)

$$\phi_{\theta,1} = \phi_{\theta,2} = \int_{k_3}^{\infty} k^{-1}\phi_{\theta,3}(k)dk \quad . \tag{8}$$

The comparison between $\phi^*_{\theta,1}(k_3^*)$ and the isotropic calculation, based on Eq. (8), is shown in Figure 6. The good agreement, almost independently of k_3^*, at the centerline (Figure 6a) contrasts with the total lack of agreement at $x_2^+ = 15$. The ratio $\phi_{\theta,1}/(\phi_{\theta,1})_{iso}$, plotted in Figure 7, suggests that, in the wall region of the flow, the anisotropy of the temperature derivative field is more pronounced than that of the vorticity field (Figure 4). This increased anisotropy may be associated with the mean temperature gradient $\overline{T}_{,2}$, where $\overline{T}$ is the mean temperature. For example, $\overline{T}_{,2}$ appears explicitly in the transport equation for the skewness of $\theta_{,1}$. Sreenivasan

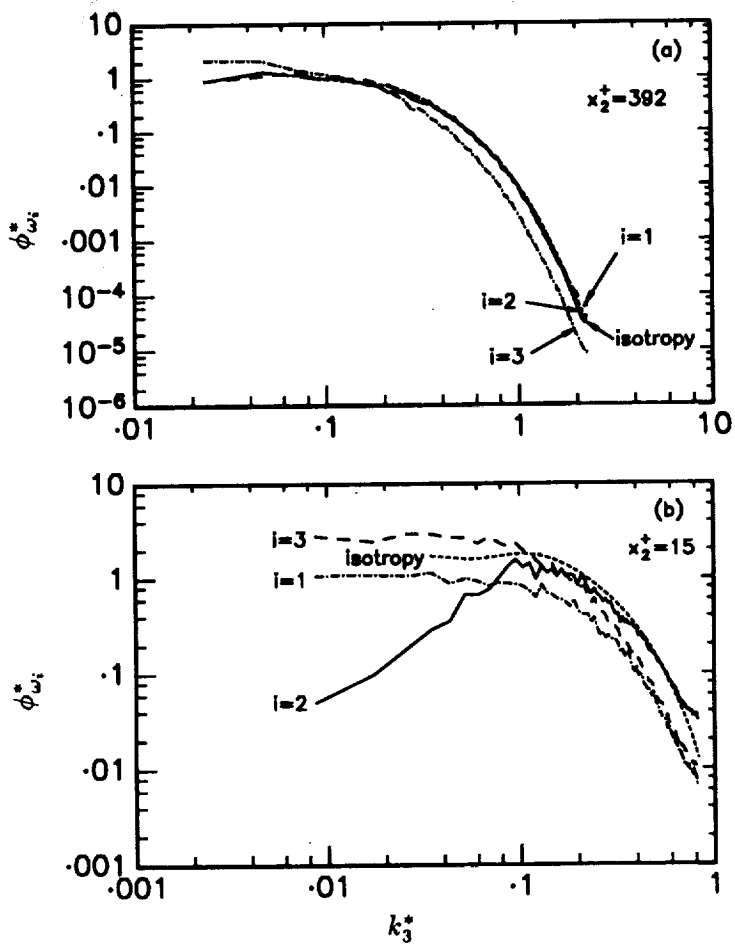

FIGURE 3. Vorticity spectra at two locations in the flow ($h^+ = 392$). (a) $x_2^+ = 392$ ($x_2 \simeq h$); (b) $x_2^+ = 15$.

and Tavoularis (1980) noted that this skewness is non-zero only when $\overline{U}_{1,2}$ and $\overline{T}_{,2}$ are both non-zero.

4 Dependence on the mean strain rate

Figures 5 and 7 suggest that the departure from isotropy may depend on the magnitude of the mean strain rate $\overline{U}_{1,2}$ ($\equiv S$). It is fairly common to normalize S by a time scale ($\overline{q^2}/2\overline{\epsilon}$) characteristic of the turbulence, e.g. Moin (1990) and Lee *et al.* (1990). Durbin and Speziale (1991) showed that the dissipation rate tensor deviates from isotropy if $S\overline{q^2}/\overline{\epsilon}$ is not zero. A disadvantage of using $S\overline{q^2}/\overline{\epsilon}$ is that it is zero at the wall where S is largest. There are other possibilities for non-dimensionalizing S. Uberoi (1957) used $S/\overline{u_{1,2}^2}^{1/2}$, with $\overline{u_{1,2}^2}^{1/2}$ representing a velocity gradient characteristic of the turbulence, for characterizing the anisotropy. Another possibility is to normalize S by the Kolmogorov time scale $(\nu/\overline{\epsilon})^{1/2}$; the ratio $S/(\overline{\epsilon}/\nu)^{1/2}$ will be

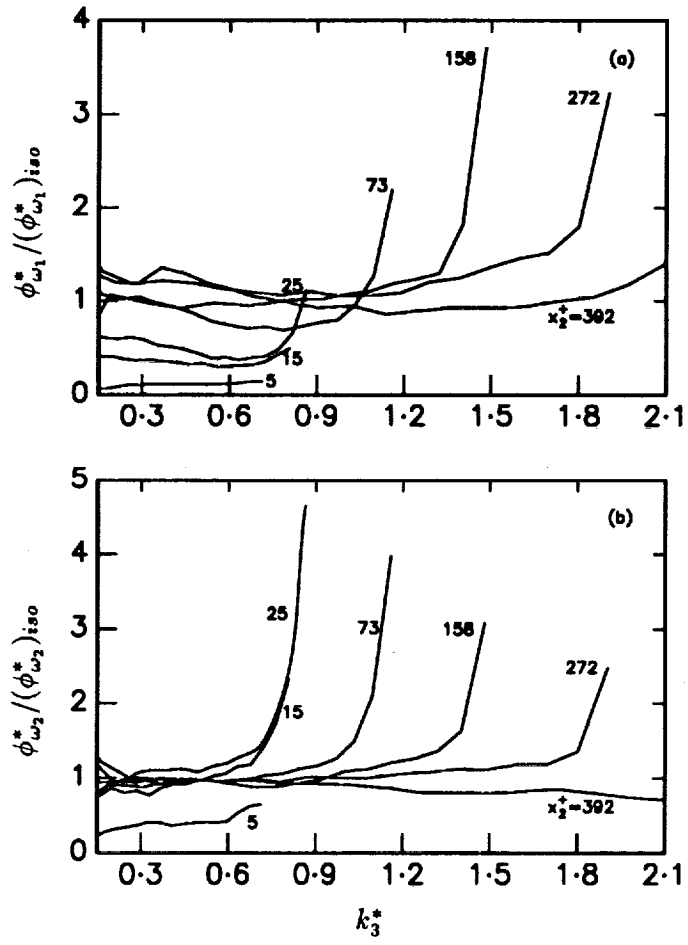

FIGURE 4. Wavenumber dependence of the ratio of the vorticity spectrum and the corresponding isotropic spectrum at different locations in the flow ($h^+ = 392$). (a) ω_1; (b) ω_2.

denoted by S^*. Corrsin (1957,1958) argued that the necessary condition for local isotropy to be a good approximation at a given wavenumber is that $(\nu/\bar{\epsilon})^{1/2}$, which may be identified with a time scale characteristic of the transfer of energy to higher wavenumbers, should be small compared with the inverse of the mean rate of strain, viz.

$$\left(\frac{\nu}{\bar{\epsilon}}\right)^{\frac{1}{2}} \ll \frac{1}{S}$$

or

$$S^* \ll 1 \quad . \tag{9}$$

The distribution of S^* is shown in Figure 8 together with $S/\overline{u_{1,2}^2}^{1/2}$ and $S\overline{q^2}/2\bar{\epsilon}$ (the corresponding distributions at $h^+ = 180$ are almost the same as those at $h^+ = 400$ in the wall region; at the wall S^* is 2.6 at $h^+ = 180$ and 2.3 at $h^+ = 400$). Not

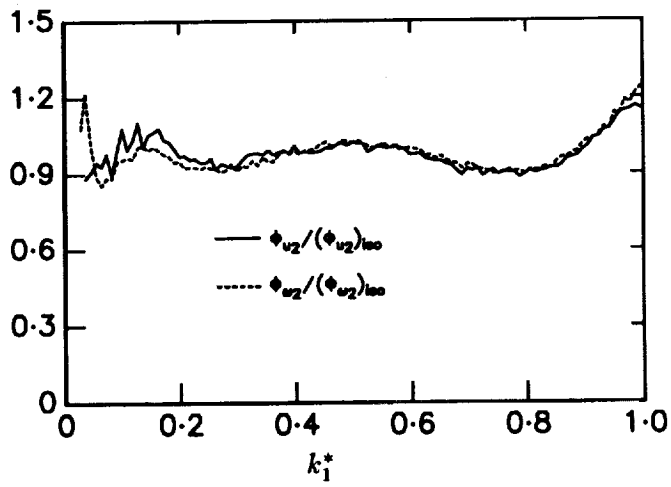

FIGURE 5. Wavenumber dependence of the ratios of spectra of u_2 and ω_2 and the corresponding isotropic spectra for a direct numerical simulation of isotropic turbulence.

unexpectedly, S^* and $S/\overline{u_{1,2}^2}^{1/2}$ follow each other closely, the former being slightly smaller than the latter in magnitude. S^* or $S/\overline{u_{1,2}^2}^{1/2}$ is clearly better behaved than $S(\overline{q^2}/2\bar{\epsilon})$, which increases from zero at the wall to a relatively large maximum near $x_2^+ = 10$.

The ratios of vorticity or temperature derivative spectra and the corresponding isotropic spectra are shown in Figure 9 in terms of S^*, for values of k_3^* in the range 0.1 to 0.7. One can identify a value of S^*, S^*_{min} say, for each of the three quantities in Figure 9 below which the ratio can be assumed to be approximately 1 (independently of k_3^*). The magnitude of S^*_{min} is about 0.3 for ω_1 while it is almost 1 for ω_2. It is only 0.1 for $\theta_{,1}$; in this case, the departure from isotropy is more evident than for vorticity, especially at smaller values of k_3^*. It would appear that while Corrsin's inequality (9) has general validity, significant relaxation of this criterion is possible when the interest centers on specific quantities. For example, it seems that $S^* \leq S^*_{min} \simeq 0.2$ may be sufficient for the small scale vorticity to be isotropic.

A comment about the possible effect of Reynolds number seems à propos here. The evidence we have gathered here and in a previous paper (Antonia *et al.*, 1991) strongly suggests that provided $S^* \lesssim S^*_{min}$, the magnitude of the Reynolds number should have little effect on the degree of isotropy that can be achieved at sufficiently large wavenumbers. The magnitude of the Reynolds number is, of course, important in determining the extent of the flow region in which $S^* \lesssim S^*_{min}$ is satisfied. This can be illustrated by reference to the logarithmic region for which energy equilibrium ($\bar{\epsilon} = -\overline{u_1 u_2} S$) is a reasonable approximation. At sufficiently high Reynolds numbers, $S \simeq U_\tau/\kappa$ (κ is the von Kármán constant, U_τ is the friction velocity), $-\overline{u_1 u_2} \simeq U_\tau^2$ and $S^* \simeq (\kappa x_2^+)^{-1/2}$. For $S^* \simeq 0.2$, this suggests that the region

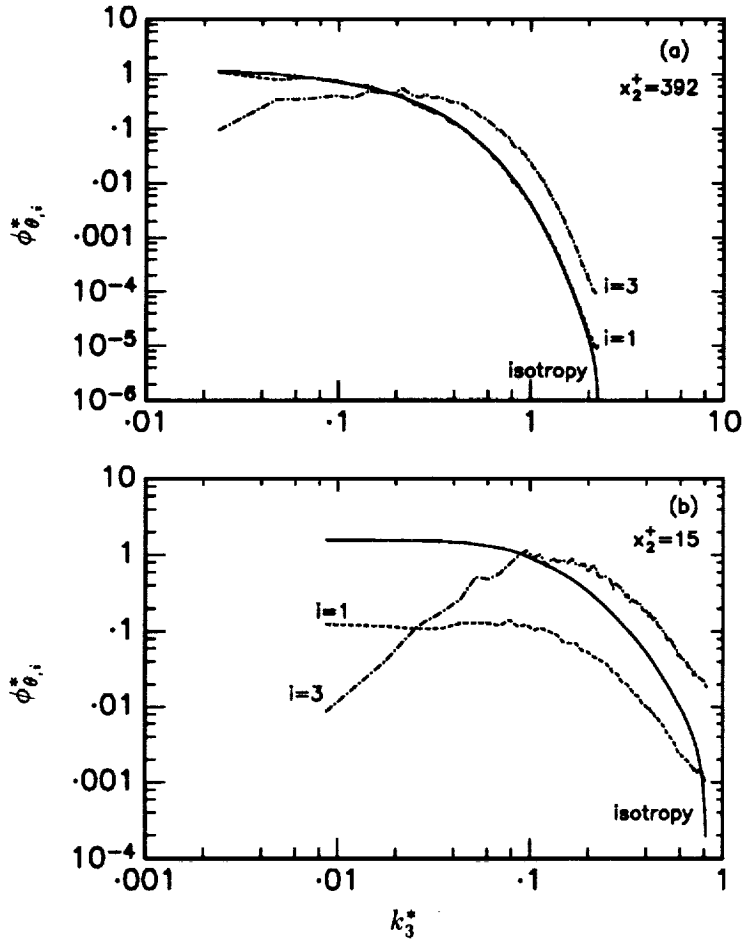

FIGURE 6. Temperature derivative spectra at two locations in the flow ($h^+ = 392$). (a) $x_2^+ = 392$; (b) $x_2^+ = 15$.

$x_2^+ \gtrsim 60$ should satisfy local isotropy; obviously, the physical extent of this region should increase with Reynolds number.

Corrsin (1957,1958) argued that a necessary condition for local isotropy is given by the inequality

$$\frac{1}{\eta} \gg \frac{S}{\overline{u_2^2}^{1/2}} \quad , \tag{10}$$

where the right side can be identified with a wavenumber, k_p say, corresponding to the turbulent energy production. The present data suggest that in the region where local isotropy is approximately satisfied, $k_p^* \lesssim 0.1$, suggesting that (10), like inequality (9), are unnecessarily restrictive and may be relaxed significantly.

5 Conclusions

Invariant maps of vorticity and temperature derivative anisotropy tensors in a

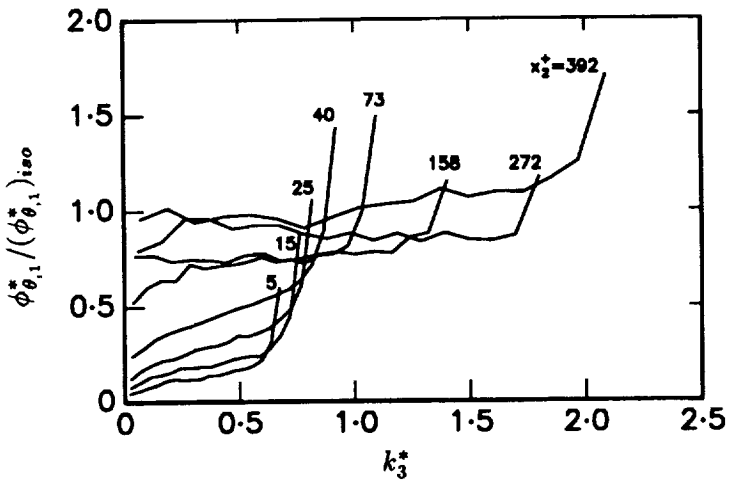

FIGURE 7. Wavenumber dependence of the ratio of the spectrum of $\theta_{,1}$ and the corresponding isotropic spectrum at different flow locations ($h^+ = 392$).

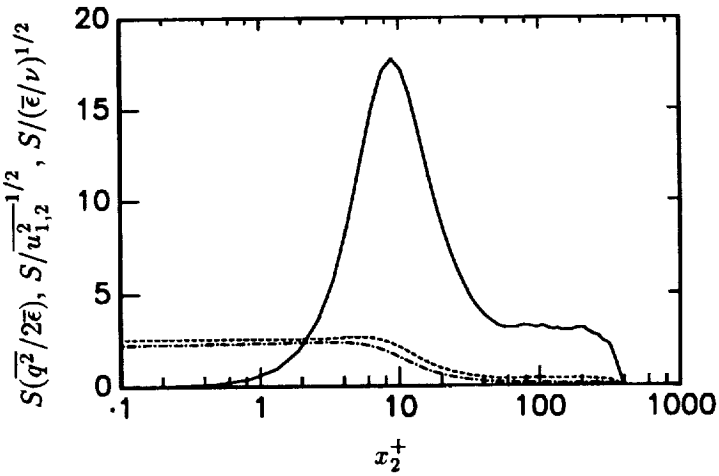

FIGURE 8. Local mean strain rate, using different normalizations ($h^+ = 392$). ——, $S(\overline{q^2}/2\overline{\epsilon})$; ----, $S/\overline{u_{1,2}^2}^{1/2}$; —·—, $S/(\overline{\epsilon}/\nu)^{1/2}$.

fully developed turbulent channel flow indicate a similar approach towards isotropy as the channel centerline is approached. In the wall region, the nature of the anisotropy is different for these two quantities.

For sufficiently large wavenumbers, vorticity and temperature derivative spectra appear to satisfy isotropy provided the mean strain rates (suitably normalized) is sufficiently small. As far as we can ascertain, this conclusion appears to be independent of the Reynolds number. Using the Kolmogorov time scale to normalize the strain rate, the value of S^* at which the departure from isotropy is first observed

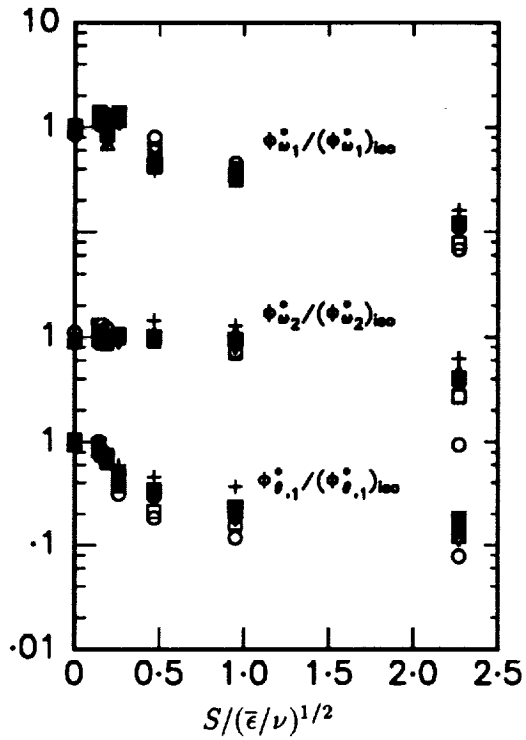

FIGURE 9. Dependence on the Kolmogorov normalized strain rate of the ratio of the vorticity or temperature derivative spectra and the corresponding isotropic spectra for different values of the wavenumber ($h^+ = 392$). (a) ω_1; (b) ω_2; (c) $\theta_{,1}$.

depends on the quantity under consideration. This value appears to be appreciably larger for the vorticity than for the temperature derivative. For given values of S^* and of the Kolmogorov normalized wavenumber, the temperature derivative spectrum exhibits a significantly larger degree of anisotropy than the vorticity spectrum. It is possible that the additional influence of the mean temperature gradient is reflected in the stronger anisotropy of the temperature derivatives, but further work would be needed to verify this possibility.

REFERENCES

ANTONIA, R. A., ANSELMET, F. & CHAMBERS, A. J. 1986 Assessment of Local Isotropy Using Measurements in a Turbulent Plane Jet. *J. Fluid Mech.* **169,** 365-391.

ANTONIA, R. A. & KIM, J. 1992 Isotropy of the Small-Scales of Turbulence at Low Reynolds Number. *J. Fluid Mech., submitted for publication.*

ANTONIA, R. A., KIM, J. & BROWNE L. W. B. 1991 Some Characteristics of Small Scale Turbulence in a Turbulent Duct Flow. *J. Fluid Mech.*. **233,** 369-388.

BATCHELOR, G. K. 1953 *The Theory of Homogeneous Turbulence*, Cambridge, Cambridge University Press.

BRASSEUR, J. G. 1991 Comments on the Kolmogorov Hypothesis of Isotropy in the Small Scales. *Paper AIAA-91-0230, 29th Aerospace Sciences Meeting, January 7-10, 1991, Reno, Nevada.*

CORRSIN, S. 1953 Remarks on Turbulent Heat Transfer: An Account of Some Features of the Phenomenon in Fully Turbulent Regions. *Proc. Iowa Thermodynamics Symposium.*

CORRSIN, S. 1957 Some Current Problems in Turbulent Shear Flows. *Symposium on Naval Hydrodynamics, F. S. Sherman (ed.) 373-400.*

CORRSIN, S. 1958 On Local Isotropy in Turbulent Shear Flow. *Report NACA R & M 58B11.*

DOMARADZKY, J. A. & ROGALLO, R. S. 1991 Local Energy Transfer and Nonlocal Interactions in Homogeneous, Isotropic Turbulence. *Phys. Fluids A.* **2,** 413-426.

DURBIN, P. A. & SPEZIALE, C. G. 1991 Local Anisotropy in Strained Turbulence at High Reynolds Numbers. *J. Fluids Eng.*. **113,** 707-709.

KOLMOGOROV, A. N. 1941 The Local Structure of Turbulence in an Incompressible Fluid with Very Large Reynolds Numbers. *Dokl. Akad, Nauk, SSSR.* **30,** 301-305.

LEE, M. J., KIM, J. & MOIN, P. 1990 Structure of Turbulence at High Shear Rate. *J. Fluid Mech.* **216,** 561-583.

LEE, M. J. & REYNOLDS, W.C. 1985 Numerical Experiments on the Structure of Homogeneous Turbulence. *Report TF-24, Thermosciences Division, Stanford University.*

LUMLEY, J. L. & NEWMAN, G. R. 1977 The Return to Isotropy of Homogeneous Turbulence. *J. Fluid Mech.* **82,** 161-178.

MESTAYER, P. 1982 Local Isotropy and Anisotropy in a High-Reynolds-Number Turbulent Boundary Layer. *J. Fluid Mech.* **125,** 475-503.

MOIN, P. 1990 Similarity of Organized Structures in Turbulent Shear Flows. *Near-Wall Turbulence, S. J. Kline and N. H. Afgan (eds.), New York, Hemisphere, 2-6.*

MONIN, A. S. & YAGLOM, A. M. 1975 Statistical Fluid Mechanics. *Mechanics of Turbulence, Vol. 2, , J. L. Lumley (ed.) Cambridge, Mass., MIT Press.*

SREENIVASAN, K. R. 1991 On Local Isotropy of Passive Scalars in Turbulent Shear Flows. *Proc. Roy. Soc. Lond.* **A434,** 165-182.

SREENIVASAN, K. R., ANTONIA, R. A. & BRITZ, D. 1979 Local Isotropy and Large Structures in a Heated Turbulent Jet. *J. Fluid Mech.* **94,** 745-775.

SREENIVASAN, K. R. & TAVOULARIS, S. 1980 On the Skewness of the Temperature Derivative in Turbulent Flows. *J. Fluid Mech.* **101,** 783-795.

UBEROI, M. S. 1957 Equipartition of Energy and Local Isotropy in Turbulent Flows. *J. Appl. Phys.* **28**, 1165-1170.

VAN ATTA, C. W. 1977 Second-Order Spectral Local Isotropy in Turbulent Scalar Fields. *J. Fluid Mech.* **80**, 609-615.

VAN ATTA, C. W. 1991 Local Isotropy of the Smallest Scales of Turbulent Scalar and Velocity Fields. *Proc. Roy. Soc. Lond.* **A434**, 139-147.

WYNGAARD, J. C. 1969 Spatial Resolution of the Vorticity Meter and Other Hot-Wire Arrays. *J. Sci. Instrum. (J. Phys. E).* **2**, 983-987.